BJP British Journal of Pharmacology

DOI:10.1111/bph.12990
www.brjpharmacol.org

RESEARCH PAPER

Localization of sunitinib, its metabolites and its target receptors in tumour-bearing mice: a MALDI-MS imaging study

S Torok[1,2,3], A Vegvari[3,4], M Rezeli[3], T E Fehniger[3,5], J Tovari[6], S Paku[7,8], V Laszlo[2], B Hegedus[2,8], A Rozsas[1,9], B Dome[1,2,9,10] and G Marko-Varga[3,5,11]

[1]*Department of tumor Biology, National Korányi Institute of Pulmonology, Budapest, Hungary,* [2]*Division of Thoracic Surgery, Department of Surgery, Comprehensive Cancer Center, Medical University of Vienna, Vienna, Austria,* [3]*Clinical Protein Science and Imaging, Biomedical Center, Department of Biomedical Engineering,* [4]*CREATE Health, and* [5]*Center of Excellence in Biological and Medical Mass Spectrometry, Lund University, Lund, Sweden,* [6]*Department of Experimental Pharmacology, National Institute of Oncology, Budapest, Hungary,* [7]*1st Institute of Pathology and Experimental Cancer Research, Semmelweis University, Budapest, Hungary,* [8]*Tumor Progression Research Group, Hungarian Academy of Sciences-Semmelweis University, Budapest, Hungary,* [9]*Department of Thoracic Surgery, Semmelweis University and National Institute of Oncology, Budapest, Hungary,* [10]*Department of Biomedical Imaging and Image-guided Therapy, Division of Molecular and Gender Imaging, Medical University of Vienna, Vienna, Austria, and* [11]*1st Department of Surgery, Tokyo Medical University, Tokyo, Japan*

Correspondence
Balazs Dome, Translational Thoracic Oncology Lab, Department of Thoracic Surgery, Medical University of Vienna; Waehringer Guertel 18-20, A-1090 Vienna, Austria. E-mail: balazs.dome@meduniwien.ac.at
Gyorgy Marko-Varga, Clinical Protein Science and Imaging, Biomedical Center, Department of Biomedical Engineering, Lund University, BMC D13, SE-221 84 Lund, Sweden. E-mail: gyorgy.marko-varga@bme.lth.se

B. D. and G. M. V. contributed equally as senior authors to this study.

Received
26 June 2014
Revised
23 September 2014
Accepted
20 October 2014

BACKGROUND AND PURPOSE
The clinical effects of anti-angiogenic agents remain controversial. Therefore, elucidating the pharmacological properties of these compounds is a pivotal issue.

EXPERIMENTAL APPROACH
The effects of treatment with sunitinib on tumour and normal tissues of mice bearing C-26 adenocarcinoma cells were analysed by matrix-assisted laser desorption ionization MS imaging (MALDI-MSI). Expression of the key targets of sunitinib – angiogenic receptors – was studied by immunofluorescent labelling.

KEY RESULTS
MALDI-MS assays showed that sunitinib and its fragment ions were present throughout tumour and normal tissues. Major metabolites were identified in blood and solid tissues, while minor drug metabolites were detectable only in blood. Tumour growth and intratumour VEGF receptor-2 expressions were significantly reduced in sunitinib-treated mice, while the expression of the other targeted receptors, PDGF receptor -α or -β and fibroblast growth factor receptor-1, remained unaffected. Within tumour tissue, the close proximity of sunitinib metabolites to the precursor ion suggested *in situ* metabolism of the administered drug. There were intratumour areas where the signal intensity of sunitinib correlated with expression of VEGF receptor-2.

CONCLUSIONS AND IMPLICATIONS

This is the first study that demonstrates MALDI-MSI is a versatile platform to study the intratumour localization of an unlabelled anti-angiogenic drug. The combination of MALDI-MSI and immunofluorescence analysis can provide further insights into the molecular interaction of drug compounds and their targets within tumour tissue.

Abbreviations

ACN, acetonitrile; ADME, adsorption, distribution, metabolism, elimination; AGC, automatic gain control; C-26, colon-26 adenocarcinoma cell line; CYP3A4, cytochrome P450 3A4; FGFR, fibroblast growth factor receptor; FT, Fourier transform; MALDI, matrix-assisted laser desorption ionization; MSI, MS imaging; *m/z*, mass-to-charge ratio; PDGFR, PDGF receptor; RTK, receptor tyrosine kinase; RTKI, receptor tyrosine kinase inhibitor; VEGFR, VEGF receptor

Tables of Links

TARGETS	
Catalytic receptors[a]	**Enzyme**[b]
PDGFR-α, PDGF receptor α	CYP3A4
PDGFR-β, PDGF receptor β	
VEGFR-2, VEGF receptor 2	
FGFR-1, FGF receptor 1	

LIGANDS
Sunitinib

These Tables list key protein targets and ligands in this article which are hyperlinked to corresponding entries in http://www.guidetopharmacology.org, the common portal for data from the IUPHAR/BPS Guide to PHARMACOLOGY (Pawson *et al.*, 2014) and are permanently archived in the Concise Guide to PHARMACOLOGY 2013/14 ([a,b]Alexander *et al.*, 2013a,b).

Introduction

The pharmacological properties of novel drug candidates are routinely characterized during the preclinical phase of drug development. However, despite the fact that the adsorption, distribution, metabolism and elimination (ADME) of drug compounds can critically influence their therapeutic benefit, in-depth and routine determination of these parameters became the focus of research only in the last decades. Until recently, extensive ADME studies were conducted rather late in the process of drug development, mainly in phase I clinical studies. This may be one of the key factors behind the low, 11%, overall first-in-man to registration rate of novel drug candidates in the 1990s. This proportion was especially poor (5%) among drugs in the field of oncology (Kola and Landis, 2004).

The vasculature is essential for the maintenance of the necessary oxygen and nutrient supply to malignant cells during tumourigenesis (Dome *et al.*, 2007). Accordingly, starving the tumour with the inhibition of endothelial growth by anti-angiogenic agents became a widely investigated and applied treatment strategy in the last decade (Waldner and Neurath, 2012). However, both experimental and clinical results with these drugs are controversial (Amir *et al.*, 2009; Loges *et al.*, 2010; Jayson *et al.*, 2012; Moreno Garcia *et al.*, 2012; Rapisarda and Melillo, 2012; Abe and Kamai, 2013). Response to treatment often manifests itself as an increase in progression-free survival, but it rarely results in an overall survival benefit (Xiao *et al.*, 2013). Thus, evaluating the ADME of these agents is a crucial step in drug development. Besides monoclonal antibodies, receptor tyrosine kinase inhibitors (RTKIs) represent the main focus of anti-angiogenic research. Among the RTKIs, sunitinib (SU11248, Sutent®, Pfizer, New York, NY, USA) is the most widely used in clinical practice. It is a multi-target RTKI, blocking the signalling of the key angiogenic receptors, the VEGF receptors (VEGFRs), the PDGF receptors (PDGFRs) and the FGF receptors (FGFRs) (Mendel *et al.*, 2003; Sun *et al.*, 2003). Between 2006 and 2011, the Food and Drug Administration approved sunitinib for the treatment of advanced gastrointestinal stromal tumour after disease progression or intolerance to imatinib mesylate (Cananzi *et al.*, 2013), of advanced renal cell carcinoma (Choueiri, 2013) and also of progressive, undifferentiated, unresectable, locally advanced or metastatic pancreatic neuroendocrine tumour (Peng and Schwarz, 2013).

The use of MALDI-MS spectroscopic techniques in pharmacological studies dates back to the mid 1990s when *in vitro* metabolites were characterized by this technique (Chung *et al.*, 1995; Ding *et al.*, 1995; Hooker *et al.*, 1995; Gusev *et al.*, 1996). The development of matrix-assisted laser desorption ionization MS imaging (MALDI-MSI), as a method to determine the spatial distribution of drugs and their metabolites at histologically relevant resolution, was an important advance in studying drug action (Khatib-Shahidi *et al.*, 2006). Compared with other methods, which localize drugs *in situ*, such as autoradiography or PET, MALDI-MSI is label-free and can be applied to native drug structures and their metabolites within any tissue environment. Using this technology, we have recently provided evidence showing the exact tissue compartment localization of low MW drugs administered to patients (Fehniger *et al.*, 2011; Marko-Varga *et al.*, 2012). To date no imaging data on the distribution of an anti-

angiogenic agent has been reported. Taking into consideration that the anti-angiogenic effect on the tumour vessel network may influence the distribution of the anti-angiogenic drug itself, such spatial distribution data could greatly help researchers to better understand the mode of action of these agents.

In the current study, we present data on the detection and distribution of sunitinib, its metabolites and its target receptors in normal and tumour tissues of mice bearing C-26 adenocarcinoma, by MALDI-MSI and immunofluorescent imaging respectively. Our results provide the first evidence that MALDI-MSI can be used to conduct ADME studies on low MW anti-angiogenic drugs.

Materials and methods

In vivo *tumour model and treatments*

All animal care and experimental procedures complied with the animal welfare regulations of the Department of Experimental Pharmacology, National Institute of Oncology, Budapest, Hungary and were approved by the Institute (permission number: 22.1/722/3/2010). Experiments involving animals are reported in accordance with the ARRIVE guidelines (Kilkenny *et al.*, 2010; McGrath *et al.*, 2010). A total of 52 animals were used in the experiments described here.

Female Balb/C mice (10 weeks old) from our colony (National Institute of Oncology, Budapest) were maintained on a daily 12-h light/12-h dark cycle and were housed under pathogen-free conditions in microisolator cages with laboratory chow and water *ad libitum*. The mouse colon-26 adenocarcinoma cell line [C-26, CLS (Cell Line Service), Mason Research Institute, Eppelheim, Germany] was cultured in RPMI 1640 with 10% FBS and 1% penicillin/streptomycin (all from Sigma-Aldrich, Steinheim, Germany) at 37°C, 5% CO_2 in a humidified atmosphere. Groups of five mice were inoculated s.c. with 2×10^6 C-26 cells, as described recently (Manea *et al.*, 2011).

Sunitinib (LC Laboratories, Woburn, MA, USA; CAS. No. 557795-19-4) treatment began 2 weeks after tumour cell injection and was performed once daily at a dose of 100 mg·kg^{-1} *per os* with a feeding tube five times a week for 2 weeks. Sunitinib at >99% purity was suspended in 2% carboxymethylcellulose with 2 mg·mL^{-1} methyl-4-hydroxibenzoate (both from Sigma-Aldrich), while control mice received only the suspending medium. Three hours after the last treatment, peripheral blood was drawn from the canthus and the animals were killed. Tumours, livers and kidneys were removed and snap frozen by submerging the tissues into liquid nitrogen-cooled isopentane, as described previously (Dome *et al.*, 2002).

Detection of the compound and analysis of drug distribution

A MALDI LTQ Orbitrap XL mass spectrometer (Thermo Fisher Scientific, Bremen, Germany) was used both for compound characterization, drug detection in blood on MALDI target plate and tissue imaging. For compound characterization, drug was dissolved in 50% methanol (MeOH, Sigma-Aldrich) at HPLC grade (>99.8%) at 1 mg·mL^{-1} stock concentration and stored at 4°C. As matrix 7.5 mg·mL^{-1} α-cyano-4-hydroxycinnamic acid (Sigma-Aldrich) was dissolved in 50% acetonitrile (ACN; hypergrade for LC-MS; Merck, Darmstadt, Germany) and 50% water, containing 0.1% trifluoroacetic acid (Sigma-Aldrich). One microlitre of the compound solution was applied on the MALDI plate with 1 μL matrix solution. Full mass spectra were obtained using the Fourier transform (FT) analyser (Orbitrap), sampling the spots in a survey mode with positive polarity, collecting 20 experiments in a single run with 60 000 resolution. The nitrogen laser was set to 10 μJ and activated automatic gain control (AGC) was used. For MS/MS experiments the detected precursor ion was fragmentized at normal scan rate, isolating the ions with mass-to-charge ratio (*m/z*) 1.0 width. The normalized collision energy (NCE) was 40% during an activation time of 30 ms and activation Q of 0.250 was applied in centroid mode.

For detection of the compound in blood, 20 μL of the plasma sample was removed and ACN precipitation was performed. Concentration and elution of the RTKI was implemented with Pierce C18 Tips (Thermo Fisher Scientific, Rockford, IL, USA) following the manufacturer's instructions. One microlitre of the sample was applied on the MALDI plate with 1 μL matrix solution using the same instrument settings as used for the compound characterization.

For tissue drug imaging, 10 μm frozen sections were cut using a cryotome and placed on glass slides. After drying of the tissue, 0.5 mL of the matrix solution was deposited stepwise by an airbrush to avoid wetting. In order to control the spraying conditions, the position of the airbrush was kept constant. Full mass spectra were obtained using the Orbitrap mass analyser at 60 000 resolution (at *m/z* 400). Tissue sections were sampled in the 150–800 Da mass range in positive mode with 100 μm raster size. The nitrogen laser was operated at 10.0 μJ with AGC on. For MS/MS data collection, the observed sunitinib peak at *m/z* 399.218 was fragmentized at normal scan rate, with *m/z* 1.0 width isolation window, using 40% NCE, 30 ms activation time and 0.250 activation Q. The minimal signal required for MS/MS spectra generation by the linear ion trap analyser was 500 counts. Analysis of the spectra was implemented with Xcalibur v 2.0.7. software, while visualization of the drug and fragment ions was performed with the ImageQuest™ software (both from Thermo Fisher Scientific, San José, CA, USA).

Quantification of the precursor compound

For in tissue quantification, calibration curves of the drug compound were established on control tissue sections of tumour, liver and kidney from mice. Sunitinib was dissolved and diluted stepwise in 50% methanol. From each concentration, 0.5 μL was applied onto the tissue surface within the concentration range of 0.00016–2.5 μmol·mL^{-1}. Spraying and detection conditions were the same as those used for the tissue sample analysis. Calibration curves were created by Quantinetix software (ImaBiotech, Loos, France).

Analysis of target receptor and drug co-localization

For the analysis of target receptor and drug co-localization, five serial frozen sections were cut from each tumour. Section #3 was used to analyse the distribution of the RTKI by

MALDI-MSI and for haematoxylin and eosin (HE) staining (Supporting information, Figures S1 and S2). Sections #1–2 and #4–5 were labelled sequentially with either of the following primary antibodies: anti-VEGFR-2 (1:50, Cell Signaling Technology, Danvers, MA, USA; Catalogue number: 55B11), anti-PDGFR-α (1:50, Cell Signaling Technology; Catalogue number: D1E1E), anti-PDGFR-β (1:50, Cell Signaling Technology; Catalogue number: C82A3) or anti-FGFR-1 (1:50, Cell Signaling Technology; Catalogue number: D8E4). All the primary antibodies were labelled with a fluorescent secondary antibody (anti-rabbit Alexa-488, 1:1000, Cell Signaling Technology; Catalogue number: 4412). Nuclei were stained with Hoechst 33342 (Molecular Probes, Eugene, OR, USA) and tumour sections were covered with ProlongGold Antifade Reagent (20 µL, Invitrogen, Carlsbad, CA, USA; Catalogue number: P36930). Slides were scanned by TissueFAXS (TissueGnostics GmbH, Vienna, Austria) and VEGFR-2, PDGFR-α, -β and FGFR-1 expression patterns were analysed by two pathologists (BD and TF).

Data analysis

Statistical analysis was performed to evaluate the *in vivo* effects of sunitinib. Two diameters of the tumours were measured three times a week and tumour volume was calculated with the formula: width^2 × length × π / 6. Difference between the treated and the control groups in tumour volume and weight was analysed by the Mann–Whitney *U*-test. Data were considered significant when $P \leq 0.05$. Data are based on five independent experiments.

Results

Sunitinib treatment inhibits tumour growth

Syngeneic subcutaneous mouse tumour models are ideal and widely used in translational medicine studies allowing us to evaluate the efficacy of various anticancer agents including anti-angiogenic drugs (Paku *et al.*, 2011; Wong *et al.*, 2012). Therefore, we decided to compare the effect of sunitinib treatment on tumour development with measures of drug distributions within the tumours. Balb/C mice were injected s.c. with C-26 mouse colon adenocarcinoma cells and 2 weeks later were dosed daily with sunitinib over a 2 week period. Tumours and other tissues were then obtained and analysed. The mean tumour weights in the control and sunitinib-treated groups were 0.274 and 0.090 g respectively (Figure 1A; $P = 0.0635$). More importantly, a 2 week sunitinib treatment resulted in a significant ($P = 0.0159$) relative tumour growth inhibition as well (Figure 1B).

MALDI-MSI identification of sunitinib and its fragment ions

We started our MALD-MSI studies by identifying the monoisotopic mass of pure stock sunitinib compound dried as a droplet at *m/z* 399.218 (Figure 2A). Subsequent MS/MS fragmentation of the precursor ions led to the loss of the terminal diethylamino group, generating a fragment ion at *m/z* 326.1, while the presence of fragment ion at *m/z* 283.1 indicated a cleavage at the amide group (Figure 2B).

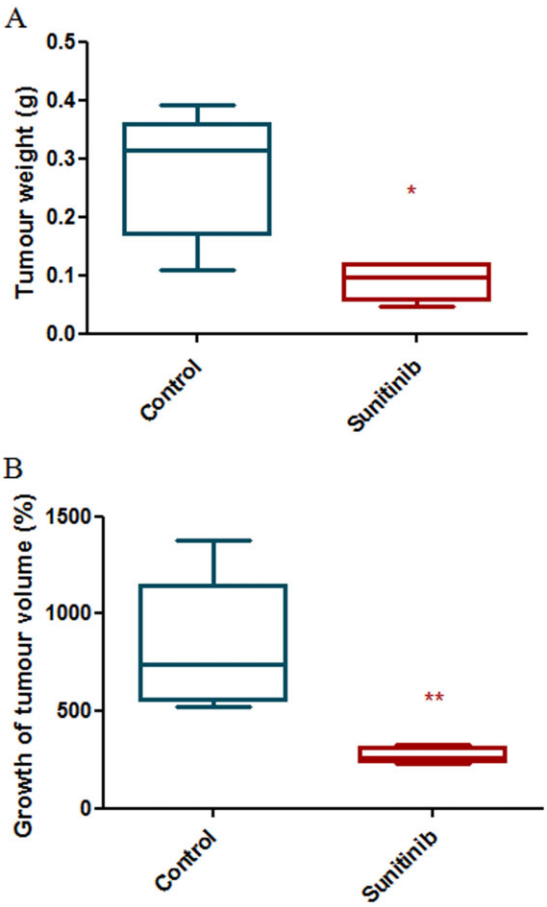

Figure 1

Sunitinib reduces the *in vivo* growth of C-26 mouse colon adenocarcinoma cells in Balb/C mice. (A) Tumour weights and (B) percentage of change of tumour volumes of control and sunitinib-treated groups (100% refers to day #1 of the treatments). Data are shown as box (first and third quartiles) and whisker (maximum to minimum) plots with the median (horizontal bar) from 5 animals per group. *P = 0.0635, **P = 0.0159, versus control.

Identification of sunitinib and its metabolites in blood

Adsorption of the drug was examined in peripheral blood. Sunitinib was measured in all plasma samples taken just before killing the animals. Moreover, metabolites of the precursor compound were also traceable and could be characterized. Presumed structures and MS/MS spectra of the precursor compound and its metabolites in blood plasma are presented in Figure 3.

The previously described bis-desethylated metabolite (M1) of sunitinib (Speed *et al.*, 2012), with a monoisotopic mass at *m/z* 343.000 could be detected only in a few blood samples performing full mass scans. However, isolating and fragmenting the proposed monoisotopic peak of that metabolite resulted in fragment ions at *m/z* 326.2 and 283.1 in all samples. Stepwise elevation of the collision energy proved that the detected fragment ions are formed by the fragmentation of M1. The missing precursor ion in full mass spectra may be explained by the low concentration of M1

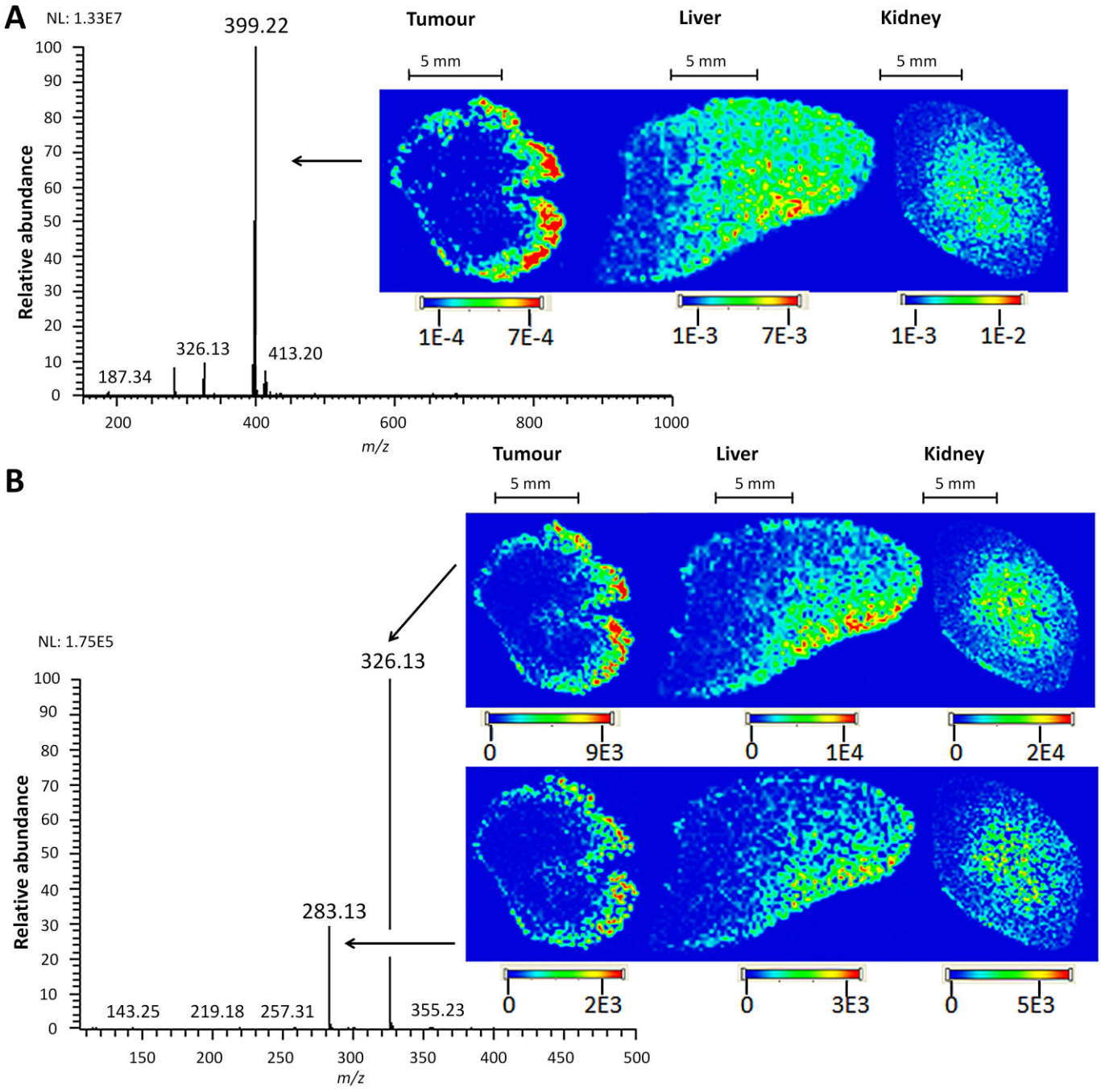

Figure 2

(A) Full mass spectrum of sunitinib and images of the distribution of the precursor molecule in tumour, liver and kidney tissues after 2 weeks of treatment. Signal of sunitinib is normalized to total ion current (TIC). (B) MS/MS spectrum of sunitinib and images of the distribution of the fragment ions (*m/z* 326.1 and 283.1) in tumour, liver and kidney tissues.

that appeared to be below the detection limit of the FT analyser compared with the linear ion trap.

The signal generated at *m/z* 358.120 of M2 indicates the loss of the terminal diethylamine group, with the oxidation of the molecule. This resulted in a fragment ion at *m/z* 283.1, but not at *m/z* 326.1. The presence of fragment ion at *m/z* 340.2 refers to the terminal dehydroxilation of the molecule.

M3, an active metabolite of sunitinib (SU012662) (Rais *et al.*, 2012) was formed by the mono-desethylation of the molecule, resulting a monoisotopic mass of *m/z* 371.188 and the same fragment ions as sunitinib.

Two mono-hydroxylated variations of the active metabolite were detected at *m/z* 387.182. M4 was modified at the indolylidene-dimethylpyrrole moiety, resulting a fragment ion at *m/z* 299.1. M5 was hydroxylated at the carbon next to

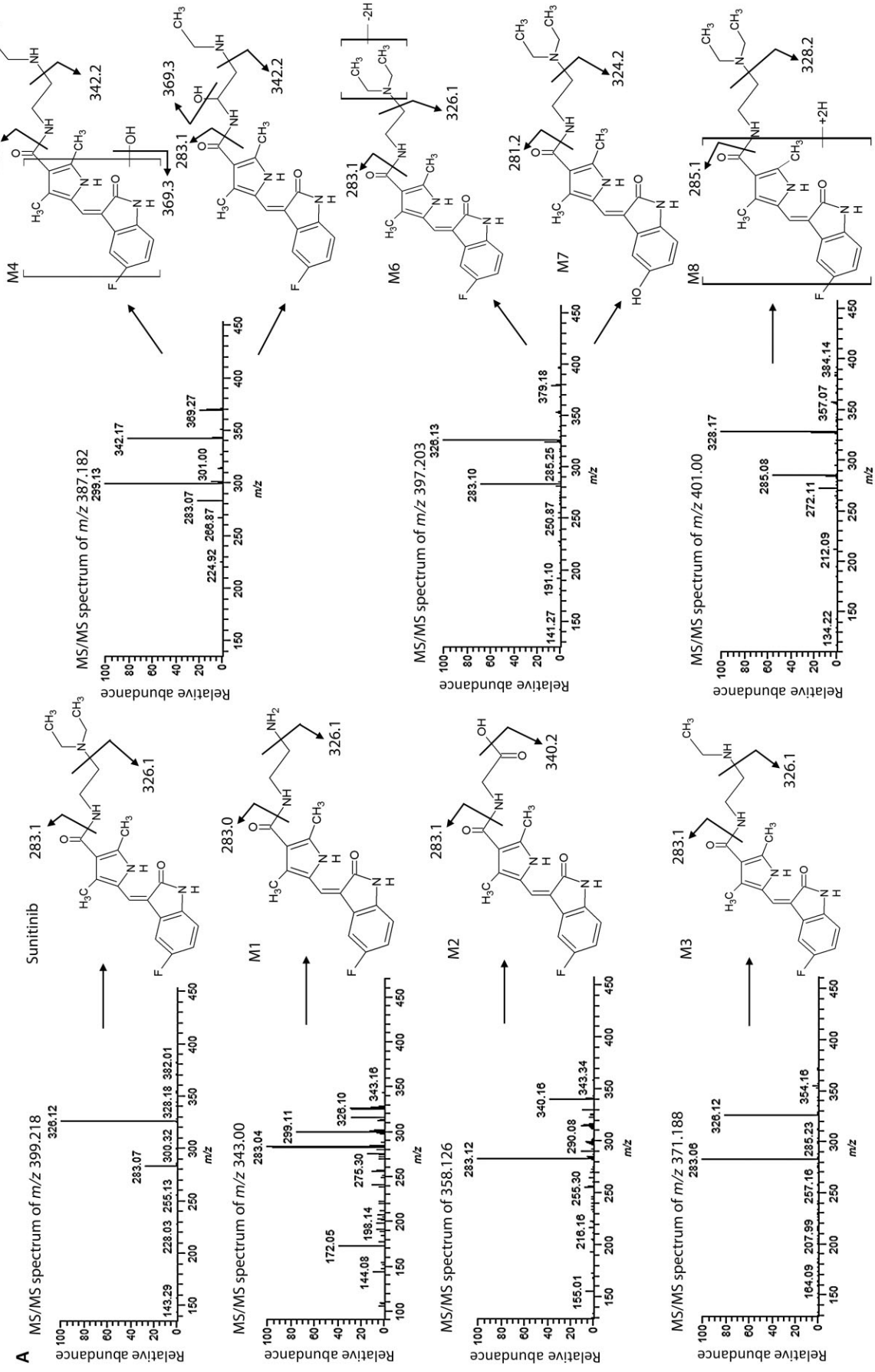

Figure 3
Detection of sunitinib and its metabolites in blood samples. MS/MS spectra of sunitinib and its metabolites (A) from *m/z* 343.00 to *m/z* 401.00 and (B) from *m/z* 415.214 to *m/z* 591.243 with the proposed structure and fragmentation properties.

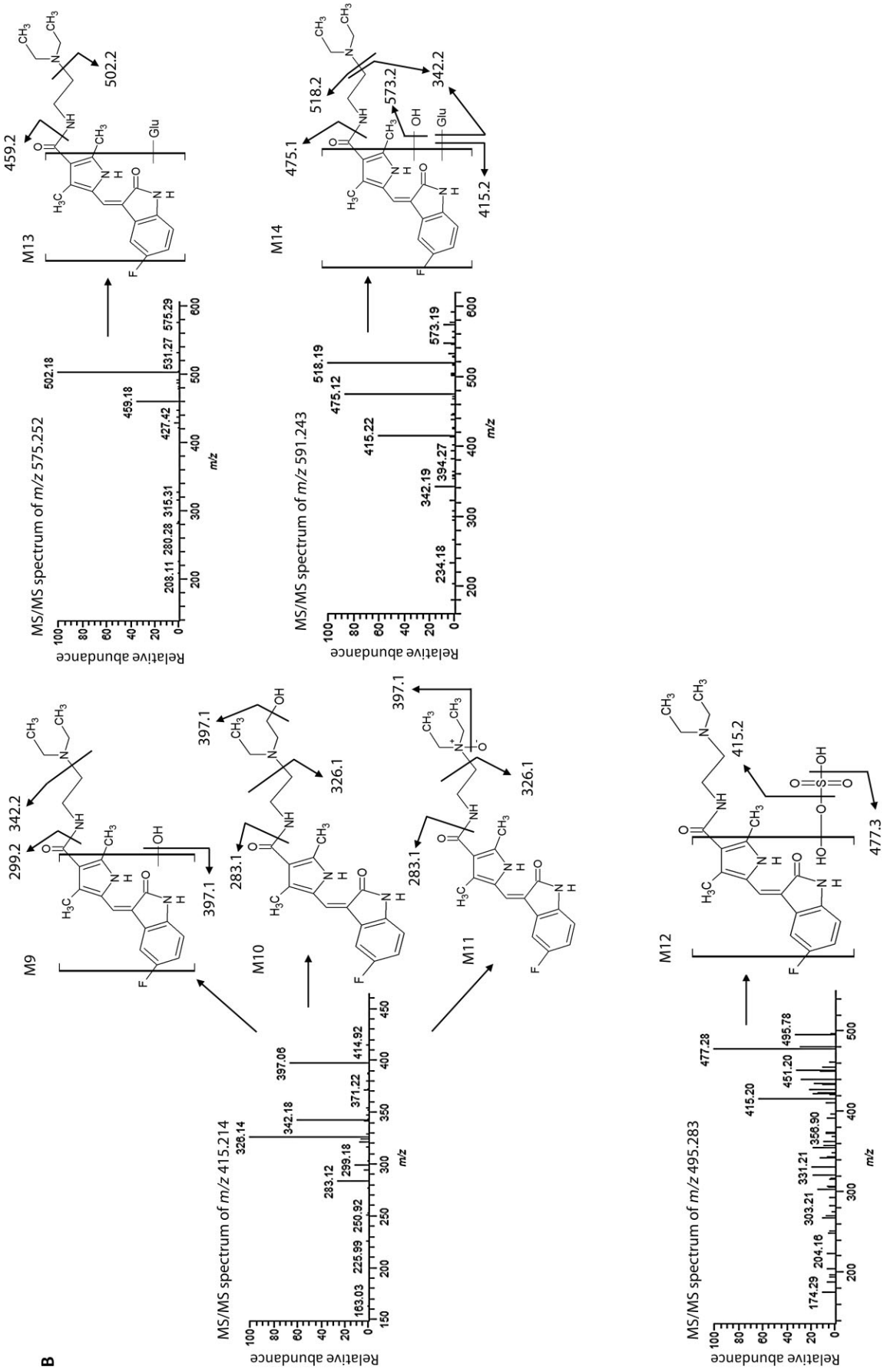

Figure 3
Continued.

the amide nitrogen, which generated a fragment ion at *m/z* 283.1. The detected fragment ion peak at *m/z* 369.1 could be derived from both molecules by dehydroxylation, such as *m/z* 342.2 by the loss of the etylamino group.

Loss of two hydrogen atoms of the terminal ethyl groups of sunitinib generated a metabolite (M6) at *m/z* 397.202. Fragmentation of the molecule generated ions at *m/z* 326.1 and 283.1.

Fragment ions of a previously described metabolite with the monoisotopic mass of *m/z* 397.224 (M7) could also be detected by MS/MS (Speed *et al.*, 2012). Signals of fragments were generated at *m/z* 324.2 and 281.2, suggesting defluorination and subsequent dehydroxylation of the molecule. M7 was not traceable by full MS, probably because of the signal suppression of M6 at *m/z* 397.202.

As with M1, the saturated metabolite of sunitinib, M8, was detected by Speed *et al.* at *m/z* 401.00 in rat and monkey faeces (Speed *et al.*, 2012). This could only be rarely measured in our mouse model by full MS. However, when isolating the presumed metabolite peak, the detected fragment ions at *m/z* 285.1 and 328.2 indicated the presence of the molecule, and that the saturation occurred at the indolylidene-dimethylpyrrole moiety.

Mono-hydroxylated metabolites of sunitinib were also measured at *m/z* 415.214. Fragmentation of the molecule indicated the oxidation on the indolylidene-dimethylpyrrole group (M9) with 16 Da higher fragments than the corresponding ions of sunitinib at *m/z* 342.2 and 299.2. Moreover, upon fragmentation of the detected metabolite peak, ions at *m/z* 326.1 and 283.1 were also formed, indicating that the oxidation occurred either at one of the terminal carbons of the diethylamine group (M10) or at the amine moiety (M11). M11 was previously synthesized as SU012487 (Speed *et al.*, 2012). Dehydroxylation of any of the mono- hydroxylated metabolites could result in a fragment ion at *m/z* 397.1.

M12 at *m/z* 495.283 was identified as a sulphate conjugate of M9. Desulphuration of the molecule gave rise to the fragment ion at *m/z* 415.2, while dehydroxylation resulted in a fragment ion at *m/z* 477.3.

The glucuronide metabolite, M13, was detected at *m/z* 575.252. The cleavage at the amide group and the loss of the terminal diethylamino moiety resulted in fragment ions at 459.2 and 502.2 respectively.

The metabolite at *m/z* 591.243 (M14) was generated by both the oxidation and the glucuronidation of sunitinib. When the molecule fragmentized as the unmodified compound, ions at *m/z* 518.2 and 475.1 were generated. Dehydroxylation eventuated in a signal at *m/z* 573.2, while the fragment ion at *m/z* 415.2 was formed by the loss of the dehydrated glucuronic acid. Deglucuronidation and dehydroxylation of the molecule resulted in an ion at *m/z* 342.2.

M3, the active metabolite generated a two- to threefold less-intensive signal than the precursor molecule in blood samples. All the other metabolites were only traceable, with less than 5% of the signal intensity of the unmodified compound (data not shown).

Distribution of administered sunitinib in tumour, liver and kidney tissue sections

The distribution of sunitinib in tumour, liver and kidney tissue samples was examined by MALDI-MSI. The precursor compound with its fragment ions could be detected in all of the tissues mentioned earlier. Representative examples showing the distribution of sunitinib and its fragment ions are shown in Figure 2. The intratumour localization of the compound was predominantly peripheral, which can either be related to the histological or to the capillary network structures of the tissues. No major intertumour heterogeneity was seen among the sunitinib-treated replicates. Sunitinib and its fragment ions showed co-localization within the tissues. This co-localization can be interpreted as a molecular fingerprint that confirms the identity of sunitinib in these measurements.

We also identified several sunitinib metabolites within the tumour tissue. In particular, the mono-desethylated (*m/z* 371.188), the desaturated (*m/z* 397.203), and the mono-hydroxylated (*m/z* 415.215) metabolites were observable by imaging (Figure 4). The precursor compound, its fragment ions and all the measured metabolites showed an overlapping tissue pattern.

Quantification of sunitinib in tumour, liver and kidney tissue samples

Quantification of the drug compound on tissue sections displayed a linear correlation between concentration and signal intensity when normalized to the matrix signal (*m/z* 379.093). This linearity was found to be between the concentration range of 0.16 nmol·mL^{-1} and 0.5 µmol·mL^{-1} in the case of liver and tumour tissues, while it was in the range of 0.16 nmol·mL^{-1} and 0.1 µmol·mL^{-1} in the case of kidney sections. The signal intensity of the manually deposited drug solution was the highest from kidney tissue and the lowest from the tumour section. Possible explanations of this phenomenon could be variations in cell density and/or in the physicochemical properties of these tissue types. Calibration curves of sunitinib obtained on tumour, liver and kidney tissue sections are shown in Figure 5.

Co-localization of drug compound and its target receptors in tumour tissue

The receptor proteins targeted by sunitininb were expressed by C-26 adenocarcinoma cells grown s.c. In these tumour cells, the patterns of expression of these targets was focal for VEGFR-2 or diffuse, for PDGFR-α, PDGFR-β and FGFR-1. Typical patterns of immunofluorescent stainings in frozen tumour tissue samples are shown in Figure 6. In line with the finding mentioned earlier that drug treatments resulted in significantly slower tumour growth *in vivo*, we also found reduced intratumour expressions of the key angiogenic receptor VEGFR-2 in sunitinib-treated animals (Figure 6A), compared with controls (Figure 6C). However, this phenomenon was not accompanied by alterations in the VEGFR-2 staining pattern, which remained focal (Figure 6A). It is also important to mention that sunitinib treatments did not affect the expression of PDGF or FGF receptors (Figure 6A).

Sunitinib was measured by MALDI-MSI by monitoring the *m/z* 399.218 ion mass, using 100 µm rastering over the entire tumour cryosection. In Figure 6B, an intensity map is shown, generated by point-by-point sampling, locating the major depots of the drug. In serial sections of sunitinib-treated tumours, the drug distribution as visualized by MALDI-MSI did not show an obvious overlap with the tissue

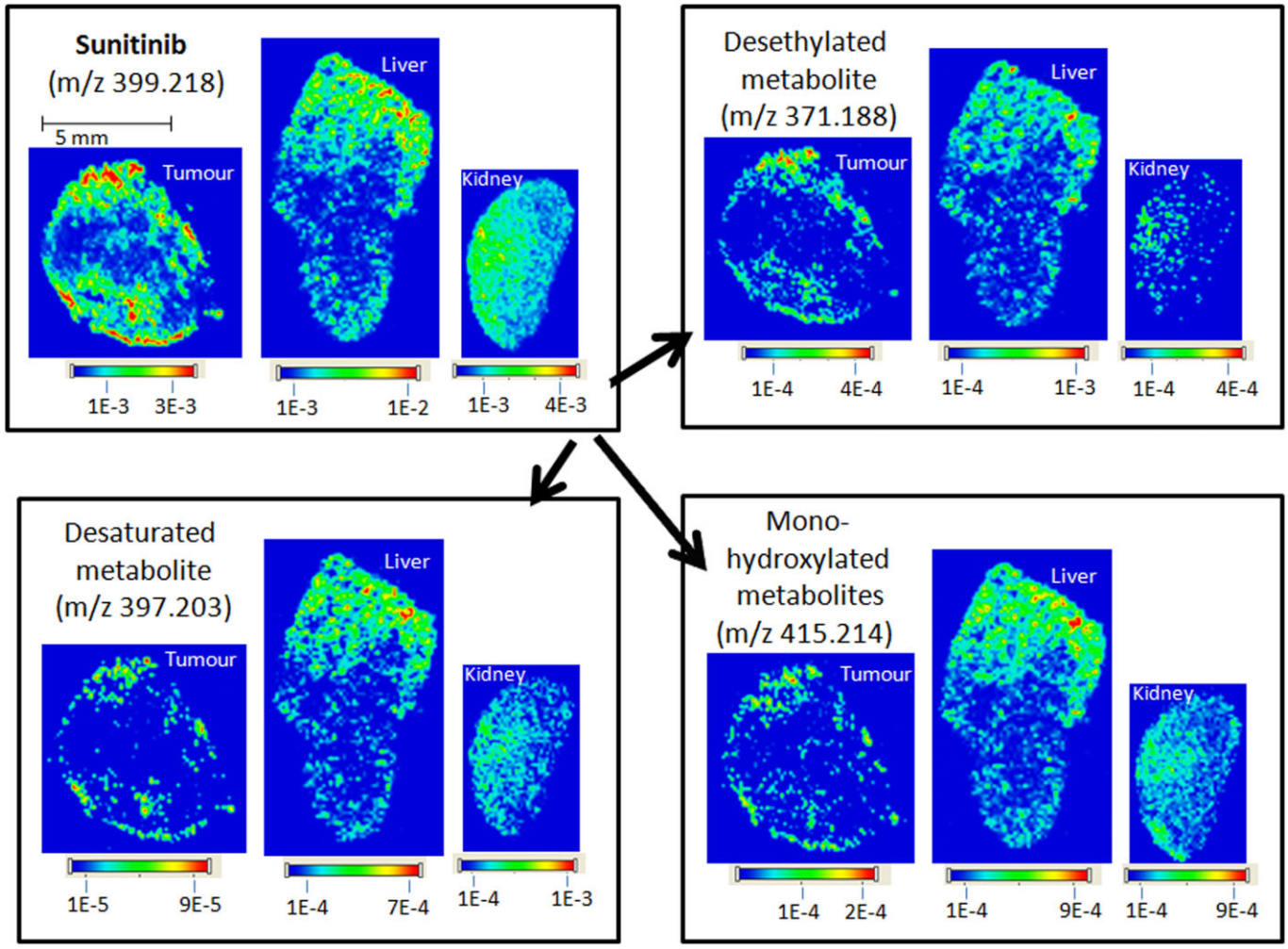

Figure 4

Distribution properties of sunitinib and its metabolites. Precursor molecule, desethylated metabolite (SU012662, M3), desaturated metabolite (M6) and mono-hydroxylated metabolites (M9, M10 and/or M11) in tumour, liver and kidney tissue sections.

labelling patterns of any of its target receptors. However, composite pictures made from the combination of MALDI-MS and immunofluorescent images identified areas where the highest concentrations of sunitinib were found in the same locations that expressed the highest concentrations of VEGFR-2 (Figure 6B). Nevertheless, this latter preliminary observation has to be confirmed by further in-depth studies.

Discussion

Sunitinib is metabolically transformed by cytochrome P450 3A4 (CYP3A4) to its active, desethylated metabolite, SU012662 (M3), which is then further modified by CYP3A4 to inactive forms (Rock *et al.*, 2007). After administration of a single oral dose, 23–37% of sunitinib is converted to SU012662 in humans (Houk *et al.*, 2010), underlining the importance of studies evaluating the metabolism of such antitumour drugs in appropriate preclinical settings. Our study confirmed that M3 is the major plasma metabolite present, not only in rats, monkeys and humans, as found by Speed *et al.* (Speed *et al.*, 2012), but also in mice. In plasma samples, the signal of this desethylated metabolite was an order of magnitude higher than that of other modified compounds. Although SU012662 generated an order of magnitude lower signal intensity in tissue than sunitinib, this was not necessarily higher than that generated by the other detectable metabolites. This observation can be explained not only by the potential difference in concentration, but also by the different ionizing properties of sunitinib and its derivatives in different tissues.

In the present study, the drug compound and its metabolites were not directly quantified. As the calibration curves we developed for this study showed linear correlation between concentration and signal intensity, such analysis could also be performed by MALDI-MSI by carefully considering the differences of signal intensities originating from different tissues. By preparing calibration curves of synthetic metabolites, accurate studies can be implemented to follow the fate of the original molecule and each of its derivatives in the body.

The observed overlap in the distribution pattern of sunitinib and its metabolites, as detected in the tissue, suggests

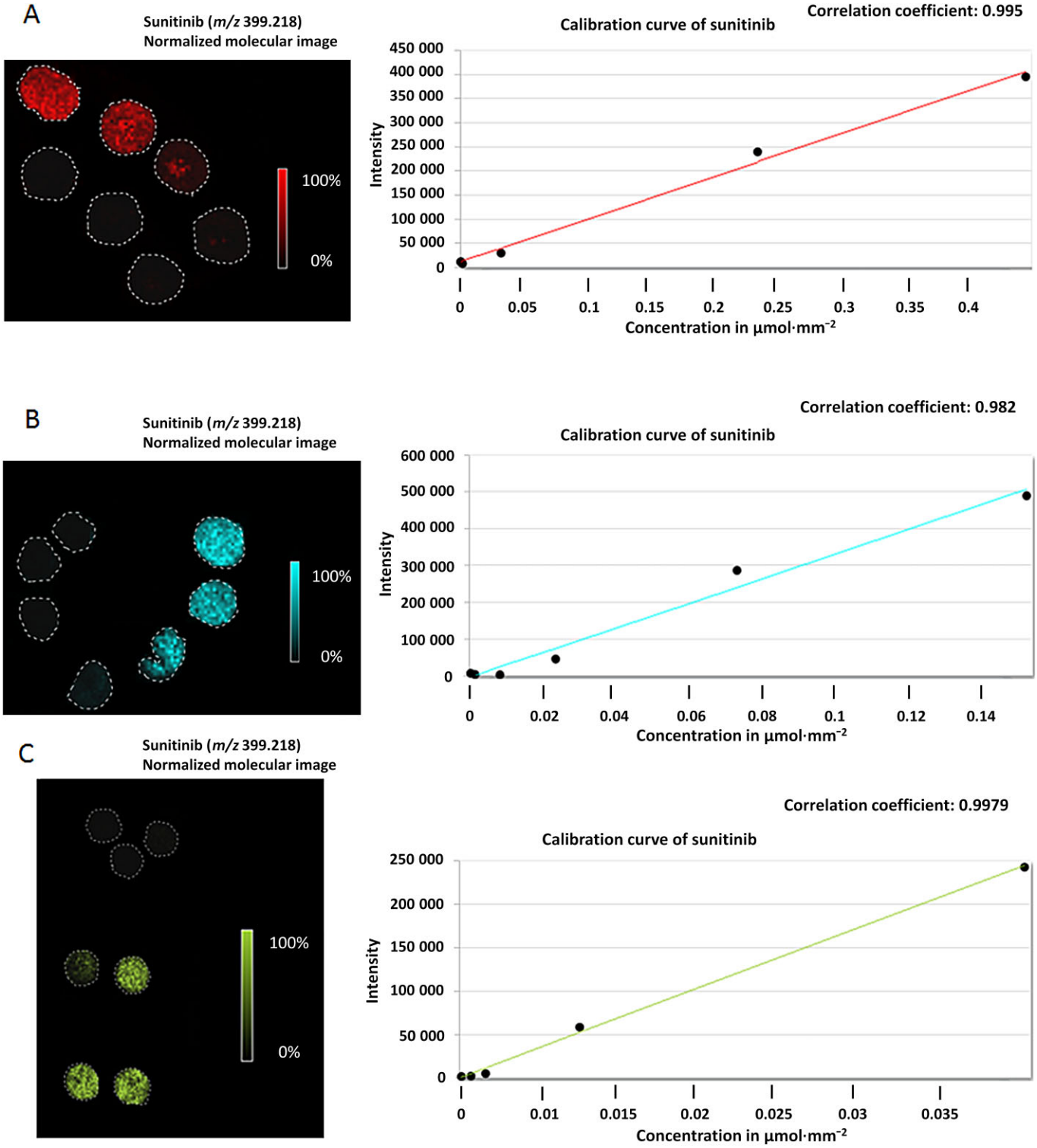

Figure 5

Quantification of sunitinib. Diagrams of MS signal intensities of sunitinib (normalized to matrix) in a concentration range of 0.064–1000 µg·mL^{-1} obtained from (A) tumour, (B) liver and (C) kidney tissue sections.

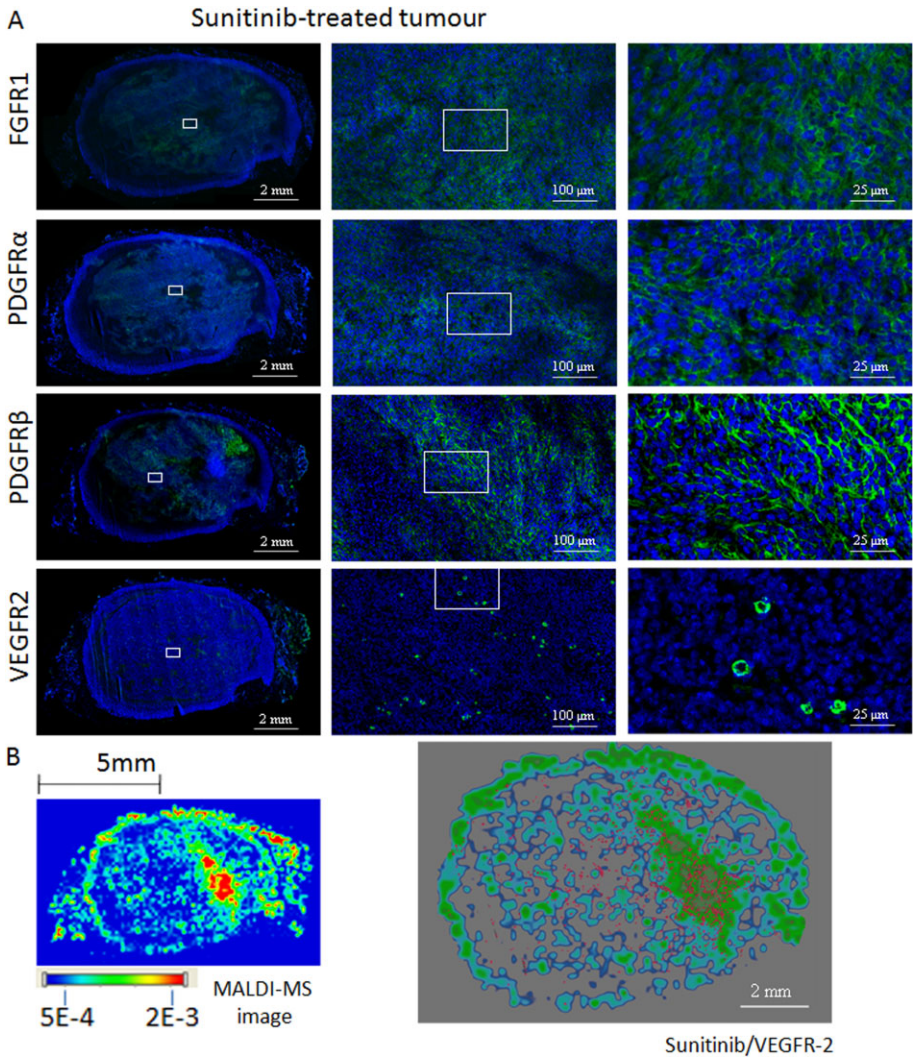

Figure 6

Intratumour distribution patterns of sunitinib and its target RTKs in sunitinib-treated (A, B) and control (C) mice as visualized by MALDI-MSI and immunofluorescent labelling respectively. In both (A) and (C), the tumours are immunolabelled for VEGFR-2, PDGFR-α, PDGFR-β and FGFR-1 (*green*). Nuclei are counterstained with Hoechst 33342 (*blue*). Note the focal (VEGFR-2) and diffuse (PDGFR-α, PDGFR-β, FGFR-1) expression patterns of the tumour cells in both animal groups. Panel B shows an example for coincidence of drug location and targeted receptor in tumour. MALDI-MSI detected sunitinib (*m/z* 399.218) at high signal intensities in the mantle and in this case in a central area as well. Signal intensity gradients of the drug were seen in discrete compartments throughout the tissue (*left picture*). In order to investigate the occurrence of cells bearing VEGFR-2 and the distribution of the drug, we first imaged the isolated VEGFR-2 signal from the RGB signal and then overlaid this image with the drug contour map. The highest density of VEGFR-2 bearing cells (*red dots*) was congruent with the highest concentrations of the drug (*right picture*). In (A) and (C), the three columns of immunofluorescent pictures (captured by a 20× objective) represent different magnifications of the same image (100, 2000 and 8000%). White rectangles in the lower-power micrographs show the corresponding areas of the higher magnification images.

that the chemical properties responsible for drug dispersion remain similar in the case of the metabolites, and accordingly, that they may contribute to the tumour growth inhibitory activity of the precursor compound as well. Alternatively, the co-localization of sunitinib and its metabolites may indicate that the drug is being taken up and metabolized locally rather than being transported from other sites of metabolism, such as the liver, back to the same location as the precursor drug. Further studies in tissue are warranted to confirm or rule out these assumptions.

Most of the techniques that have analysed sunitinib and its derivatives are based on liquid chromatography coupled with mass spectrometric detection (Baratte *et al.*, 2004; de Bruijn *et al.*, 2010; Zhou and Gallo, 2010; Lankheet *et al.*, 2011; Rodamer *et al.*, 2011; Rais *et al.*, 2012; Speed *et al.*, 2012; Qiu *et al.*, 2013). However, Etienne-Grimaldi *et al.* described an HPLC method linked to UV detection of sunitinib and SU12662 in human plasma (Etienne-Grimaldi *et al.*, 2009). The *m/z* values of the precursor drug and its derivatives in our study are consistent with these earlier results. The

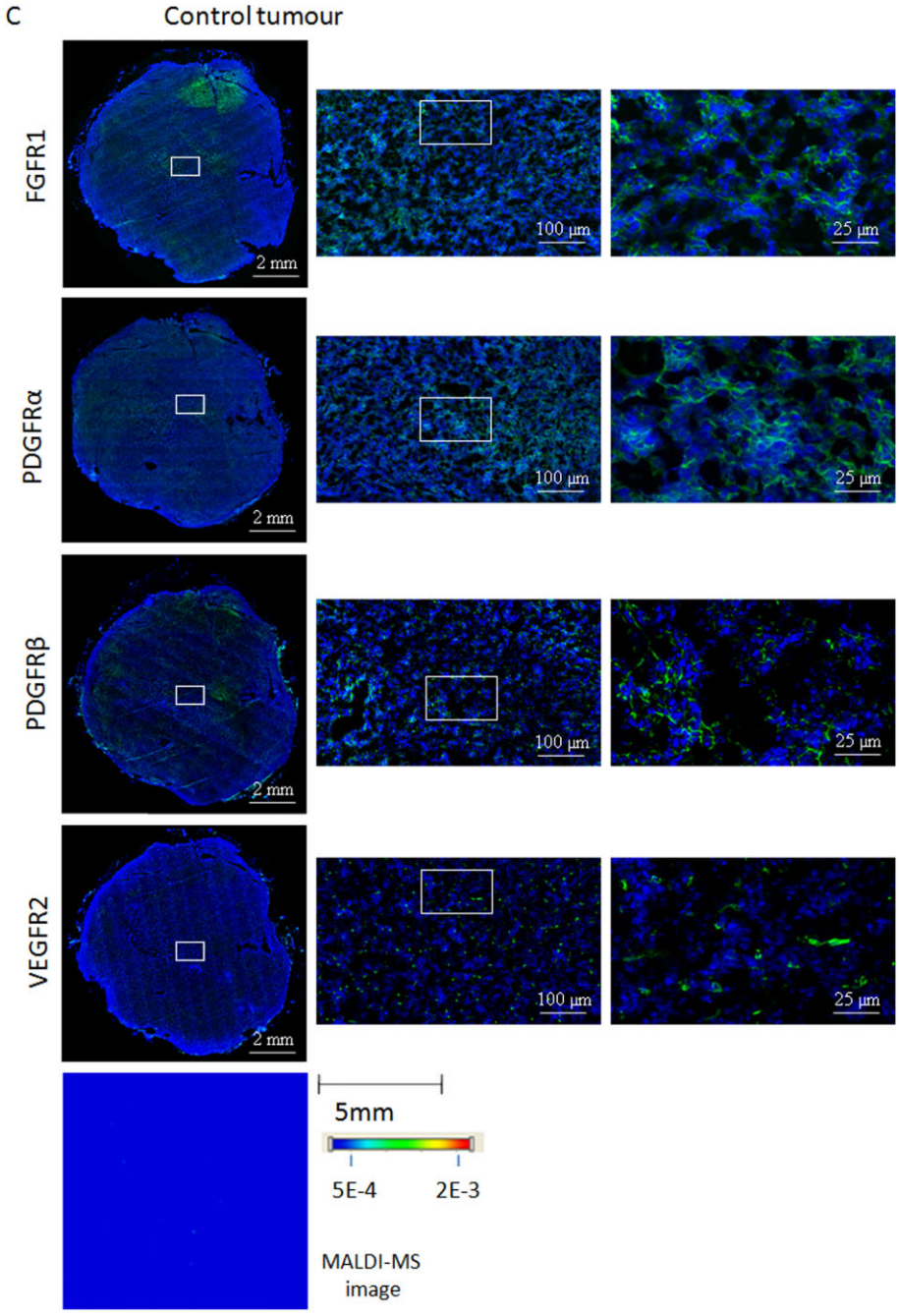

Figure 6
Continued.

present study showed that MALDI-MS is also a powerful tool to detect the drug compound ions and its metabolites. The MALDI-MS experimental parts showed a slightly different fragmentation pattern from electrospray ionization-MS (Speed *et al.*, 2012). Moreover, an advantage of MALDI-MSI compared with other previously used methods is that the earlier techniques require either fluid samples (such as blood or sweat) or the homogenization of the tissue. Therefore, they are not capable of analysing the spatial tissue distribution of a compound in an organ or in a solid tumour.

Although the last half century has witnessed dramatic advances in the field of medical imaging, there is still an urgent need for the development of more advanced techniques for imaging compounds in the drug discovery process. This is particularly important in the narrowing of the selection of potential hits and leads as candidates for further development. One of the reasons this has been difficult to accomplish in the past is that until recently, the only avenue for visualizing the *in vivo* distribution of drugs in targeted tissues was to use labels, which are commonly radioactive,

and as such a safety risk. Methods such as PET and autoradiography can provide information on the distribution of a radiolabelled compound, even at the cellular level (Solon *et al.*, 2010; Solon, 2012). However, both of these methods rely on quantitative data based upon the relative strength of the label rather than the relative concentration of the drug. For these reasons, unlabelled, that is 'cold' compounds will provide evidence that relate to the drug structure only and not to the labelling chemistry in a modified drug molecule. If a drug is metabolized such that the label follows on the fragment that is neither active, nor the precursor of an active form, then the readout of distribution may have little to do with the mode of action or the actual efficacy of the drug (Solon, 2012). Other methods rely on the use of isotopes with relatively short half-lives or fluorescent tags, which makes long-term pharmacological analysis impossible or alters the chemical structure and thus the binding affinity and/or avidity to its target molecule (Solon *et al.*, 2010).

From this point of view, it is particularly important that methods be used that investigate the characteristics of the unaltered native compound (i.e. the same agent as that being administered to patients). MS is one such powerful technique, enabling the parallel determination of label-free drugs and their metabolites. The Orbitrap mass analyser in the hybrid instrument used in our study provides very high levels of mass accuracy, to the tens of thousands fraction on a single atomic mass unit (Strupat *et al.*, 2009). This high accuracy in identification allows strong statistical support for the mass values that we have reported here for sunitinib as either precursor ions, fragment ions, or metabolites formed *in situ*. The MALDI-MSI technology also allowed label-free identification of this small molecule compound, negating the concern that drug properties could have been altered by the labelling procedure. In principle, MALDI-MSI is not limited to the analysis of low MW compounds, but it might also be suitable for the localization of therapeutic macromolecules, such as peptides (Craik *et al.*, 2013) and antibodies (Glassman and Balthasar, 2014). In practice, however, the identification of specific antibodies by MALDI-MSI is a challenge as time-of-flight instruments with broad mass range (over *m/z* 1 million) do not have sufficient resolution at high mass range, while Orbitraps operate up to *m/z* 4000 (and thus unable to detect singly charged peptides over 4 kDa). Enzymic *in situ* digestion (Groseclose *et al.*, 2007; Casadonte and Caprioli, 2011; Gustafsson *et al.*, 2013) may provide unique peptides that can help in their precise localization within tissue sections. However, the identification of these peptides is still restricted to matching the accurate precursor masses in MALDI-MS analysis with those observed in an LC-MS/MS experiment used for peptide sequencing.

The current study is the first describing the tissue distribution of an unlabelled anti-angiogenic RTKI and its metabolites by MSI. In our study, the combination of the resolving power of the Orbitrap with the sensitivity of the linear ion trap made it an ideal technique for drug and metabolite detection. We observed that oral administration of sunitinib resulted in a systemic distribution of the drug throughout the body with significant levels being observed in the blood, liver, kidneys and tumour tissue. In this study, we have investigated the patterns of drug distribution in the animals following 2 weeks of daily sunitinib dosing. As such, we have not studied the kinetics of drug accumulation in specific tissue sites, or the kinetics of changes in the biological/histological makeup of the tumours throughout the course of treatment. We have clearly shown that sunitinib-treated tumours showed areas of higher (typically peripheral) and lower (tumour centre) drug signal intensities rather than a homogeneous dispersal across the entire tumour. Of note, this distribution pattern (i.e. higher signal intensity at the tumour periphery vs. relatively lower levels in the central tumour regions) proved to be reproducible throughout the drug-treated tumour sample replicates. In accordance with the findings of Domingues *et al.*, we observed that VEGFR-2 expression was significantly reduced in treated tumours, compared with untreated ones (Domingues *et al.*, 2011). The relationship between this reduction and the exposure to the drug cannot be investigated in this study because of a single time point of analysis. However, we can say that the time point represented a window showing a clear biological effect of the drug treatment, as seen by both a reduction in tumour weight and volume.

Today, our understanding of the mode of action and the efficacy of antivascular agents in oncology is especially complex and peculiar. Accordingly, when interpreting our findings, we need to take into consideration that both the tumour tissue levels of sunitininb and the expression pattern of its target receptors vary both spatially and temporally. The actual tumour tissue level of an anticancer drug is always influenced by the global blood supply of the tumour mass and also by local intratumour blood flow changes (i.e. by the distinct vascularization patterns of different intratumour areas as well). Although they also have direct effect against autocrine tumour cell signalling, the main effect of antivascular agents (such as sunitinib) is exerted on the tumour vasculature itself and, consequently, sunitinib influences the efficacy of its own delivery. Additional key background information is that sunitinib binds to its target receptors reversibly and, moreover, that it may also result in significant changes in the expression levels and patterns of its target receptors (Roskoski, 2007). Our approach can contribute to the elucidation of this complex biology in order to further develop anti-angiogenic treatment strategies.

To the best of our knowledge, the current study provides the first direct evidence that an anti-angiogenic drug given orally is transported to, taken up and metabolized within the targeted compartment, the adenocarcinoma tumour. Moreover, the presented results are the first demonstrating that MALDI-MSI is a versatile and simple method of conducting ADME studies on an anti-angiogenic RTKI. Hence, the current study warrants further investigations to define the precise and optimal role of MALDI-MSI in elucidating the mechanisms of drug action and for validating transport to sites of intended effect.

Acknowledgements

The authors were supported by Kutatási és Technológiai Innovációs Alap (Research and Technology Innovation Fund) AIK 12-1-2013-0041 (B. D., V. L., S. P.); Országos Kutatási Tudományos Alapprogramok (Hungarian Scientific Research Fund) K109626, K108465 (B. D., B. H.), MOB80325 (B. H.),

and K84173 (J. T.); EUREKA_HU_12-1-2012-0057 (B. D.); ÖNB Jubiläumsfondsprojekt No. 14043 (B. D., V. L.); and the Vienna Fund for Innovative Interdisciplinary Cancer Research (B. D., V. L.). S. T. was recipient of an EACR Travel Fellowship and a Hungarian Pulmonology Foundation Research Fellowship. A. V. is grateful for the Innovative Support 2011-039226 for CREATE Health. This work was also supported by grants from the Mrs. Berta Kamprad Foundation, Ingabritt & Arne Lundbergs forskningsstiftelse and the Crafoord Foundation.

Author contributions

S. T. was responsible for the implementation of the animal experiment, for the immunohistochemical and MALDI data acquisition. She contributed in the preparation of the paper. A. V. was responsible for the MALDI-MS data analysis and interpretation, and was also involved in the preparation of the paper. M. R. was involved in the MALDI-MS data acquisition and analysis. T. E. F. was responsible for the immunohistochemical data analysis and interpretation. He was also involved in the preparation of the paper. J. T. was responsible for the design and data analysis of the *in vivo* animal experiment. S. P. was responsible for the design and expertise of the immunohistochemical part of the project. V. L. and A. R. were responsible for the scanning of the immunolabelled and HE-stained slides.

B. H. was involved in the preparation of the paper. B. D. was responsible for the study design, analysis of the immunohistochemical data and for data interpretation. He was also involved in the preparation of the paper. G. M. V. was responsible for the design of the MALDI-MS experimental part, for drafting the paper and for coordinating and overseeing the project.

Conflict of interest

Authors declare no conflict of interest. The funders had no role in study design, data collection and analysis, decision to publish or preparation of the paper.

References

Abe H, Kamai T (2013). Recent advances in the treatment of metastatic renal cell carcinoma. Int J Urol 20: 944–955.

Alexander SPH, Benson HE, Faccenda E, Pawson AJ, Sharman JL Spedding M *et al.* (2013a). The Concise Guide to PHARMACOLOGY 2013/14: Catalytic Receptors. Br J Pharmacol 170, 1676–1705.

Alexander SPH, Benson HE, Faccenda E, Pawson AJ, Sharman JL Spedding M *et al.* (2013b). The Concise Guide to PHARMACOLOGY 2013/14: Enzymes. Br J Pharmacol 170: 1797–1867

Amir E, Mandoky L, Blackhall F, Thatcher N, Klepetko W, Ankersmit HJ *et al.* (2009). Antivascular agents for non-small-cell lung cancer: current status and future directions. Expert Opin Investig Drugs 18: 1667–1686.

Baratte S, Sarati S, Frigerio E, James CA, Ye C, Zhang Q (2004). Quantitation of SU1 1248, an oral multi-target tyrosine kinase inhibitor, and its metabolite in monkey tissues by liquid chromatograph with tandem mass spectrometry following semi-automated liquid-liquid extraction. J Chromatogr A 1024: 87–94.

de Bruijn P, Sleijfer S, Lam MH, Mathijssen RH, Wiemer EA, Loos WJ (2010). Bioanalytical method for the quantification of sunitinib and its n-desethyl metabolite SU12662 in human plasma by ultra performance liquid chromatography/tandem triple-quadrupole mass spectrometry. J Pharm Biomed Anal 51: 934–941.

Cananzi FC, Judson I, Lorenzi B, Benson C, Mudan S (2013). Multidisciplinary care of gastrointestinal stromal tumour: a review and a proposal for a pre-treatment classification. Eur J Surg Oncol 39: 1171–1178.

Casadonte R, Caprioli RM (2011). Proteomic analysis of formalin-fixed paraffin-embedded tissue by MALDI imaging mass spectrometry. Nat Prot 6: 1695–1709.

Choueiri TK (2013). Clinical treatment decisions for advanced renal cell cancer. J Natl Compr Canc Netw 11: 694–697.

Chung WG, Miranda CL, Buhler DR (1995). A cytochrome P4502B form is the major bioactivation enzyme for the pyrrolizidine alkaloid senecionine in guinea pig. Xenobiotica 25: 929–939.

Craik DJ, Fairlie DP, Liras S, Price D (2013). The future of peptide-based drugs. Chem Biol Drug Des 81: 136–147.

Ding A, Zia-Amirhosseini P, McDonagh AF, Burlingame AL, Benet LZ (1995). Reactivity of tolmetin glucuronide with human serum albumin. Identification of binding sites and mechanisms of reaction by tandem mass spectrometry. Drug Metab Dispos 23: 369–376.

Dome B, Paku S, Somlai B, Timar J (2002). Vascularization of cutaneous melanoma involves vessel co-option and has clinical significance. J Pathol 197: 355–362.

Dome B, Hendrix MJ, Paku S, Tovari J, Timar J (2007). Alternative vascularization mechanisms in cancer: pathology and therapeutic implications. Am J Pathol 170: 1–15.

Domingues I, Rino J, Demmers JA, de Lanerolle P, Santos SC (2011). VEGFR2 translocates to the nucleus to regulate its own transcription. PLoS ONE 6: e25668.

Etienne-Grimaldi MC, Renee N, Izzedine H, Milano G (2009). A routine feasible HPLC analysis for the anti-angiogenic tyrosine kinase inhibitor, sunitinib, and its main metabolite, SU12662, in plasma. J Chromatogr B Analyt Technol Biomed Life Sci 877: 3757–3761.

Fehniger TE, Vegvari A, Rezeli M, Prikk K, Ross P, Dahlback M *et al.* (2011). Direct demonstration of tissue uptake of an inhaled drug: proof-of-principle study using matrix-assisted laser desorption ionization mass spectrometry imaging. Anal Chem 83: 8329–8336.

Glassman PM, Balthasar JP (2014). Mechanistic considerations for the use of monoclonal antibodies for cancer therapy. Cancer Biol Med 11: 20–33.

Groseclose MR, Andersson M, Hardesty WM, Caprioli RM (2007). Identification of proteins directly from tissue: *in situ* tryptic digestions coupled with imaging mass spectrometry. J Mass Spectrom 42: 254–262.

Gusev AI, Muddiman DC, Proctor A, Sharkey AG, Hercules DM, Tata PN *et al.* (1996). A quantitative study of *in vitro* hepatic metabolism of tacrolimus (FK506) using secondary ion and matrix-assisted laser desorption/ionization mass spectrometry. Rapid Commun Mass Spectrom 10: 1215–1218.

Gustafsson OJ, Eddes JS, Meding S, McColl SR, Oehler MK, Hoffmann P (2013). Matrix-assisted laser desorption/ionization imaging protocol for *in situ* characterization of tryptic peptide identity and distribution in formalin-fixed tissue. Rapid Commun Mass Spectrom 27: 655–670.

Hooker AD, Goldman MH, Markham NH, James DC, Ison AP, Bull AT *et al.* (1995). N-glycans of recombinant human interferon-gamma change during batch culture of Chinese hamster ovary cells. Biotechnol Bioeng 48: 639–648.

Houk BE, Bello CL, Poland B, Rosen LS, Demetri GD, Motzer RJ (2010). Relationship between exposure to sunitinib and efficacy and tolerability endpoints in patients with cancer: results of a pharmacokinetic/pharmacodynamic meta-analysis. Cancer Chemother Pharmacol 66: 357–371.

Jayson GC, Hicklin DJ, Ellis LM (2012). Antiangiogenic therapy – evolving view based on clinical trial results. Nat Rev Clin Oncol 9: 297–303.

Khatib-Shahidi S, Andersson M, Herman JL, Gillespie TA, Caprioli RM (2006). Direct molecular analysis of whole-body animal tissue sections by imaging MALDI mass spectrometry. Anal Chem 78: 6448–6456.

Kilkenny C, Browne W, Cuthill IC, Emerson M, Altman DG, Group NCRRGW (2010). Animal research: reporting *in vivo* experiments: the ARRIVE guidelines. Br J Pharm 160: 1577–1579.

Kola I, Landis J (2004). Can the pharmaceutical industry reduce attrition rates? Nat Rev Drug Discov 3: 711–715.

Lankheet NA, Blank CU, Mallo H, Adriaansz S, Rosing H, Schellens JH *et al.* (2011). Determination of sunitinib and its active metabolite N-desethylsunitinib in sweat of a patient. J Anal Toxicol 35: 558–565.

Loges S, Schmidt T, Carmeliet P (2010). Mechanisms of resistance to anti-angiogenic therapy and development of third-generation anti-angiogenic drug candidates. Genes Cancer 1: 12–25.

Manea M, Leurs U, Orban E, Baranyai Z, Ohlschlager P, Marquardt A *et al.* (2011). Enhanced enzymatic stability and antitumor activity of daunorubicin-GnRH-III bioconjugates modified in position 4. Bioconjug Chem 22: 1320–1329.

Marko-Varga G, Vegvari A, Rezeli M, Prikk K, Ross P, Dahlback M *et al.* (2012). Understanding drug uptake and binding within targeted disease micro-environments in patients: a new tool for translational medicine. Clin Transl Med 1: 8.

McGrath J, Drummond G, Kilkenny C, Wainwright C (2010). Guidelines for reporting experiments involving animals: the ARRIVE guidelines. Br J Pharmacol 160: 1573–1576.

Mendel DB, Laird AD, Xin X, Louie SG, Christensen JG, Li G *et al.* (2003). *In vivo* antitumor activity of SU11248, a novel tyrosine kinase inhibitor targeting vascular endothelial growth factor and platelet-derived growth factor receptors: determination of a pharmacokinetic/pharmacodynamic relationship. Clin Cancer Res 9: 327–337.

Moreno Garcia V, Basu B, Molife LR, Kaye SB (2012). Combining antiangiogenics to overcome resistance: rationale and clinical experience. Clin Cancer Res 18: 3750–3761.

Paku S, Dezso K, Bugyik E, Tovari J, Timar J, Nagy P *et al.* (2011). A new mechanism for pillar formation during tumor-induced intussusceptive angiogenesis: inverse sprouting. Am J Pathol 179: 1573–1585.

Pawson AJ, Sharman JL, Benson HE, Faccenda E, Alexander SP, Buneman OP *et al.*; NC-IUPHAR (2014). The IUPHAR/BPS Guide to PHARMACOLOGY: an expert-driven knowledge base of drug targets and their ligands. Nucl. Acids Res. 42 (Database Issue): D1098–1106.

Peng L, Schwarz RE (2013). Pancreatic neuroendocrine tumors: signal pathways and targeted therapies. Curr Mol Med 13: 333–339.

Qiu F, Bian W, Li J, Ge Z (2013). Simultaneous determination of sunitinib and its two metabolites in plasma of Chinese patients with metastatic renal cell carcinoma by liquid chromatography-tandem mass spectrometry. Biomed Chromatogr 27: 615–621.

Rais R, Zhao M, He P, Xu L, Deeken JF, Rudek MA (2012). Quantitation of unbound sunitinib and its metabolite N-desethyl sunitinib (SU12662) in human plasma by equilibrium dialysis and liquid chromatography-tandem mass spectrometry: application to a pharmacokinetic study. Biomed Chromatogr 26: 1315–1324.

Rapisarda A, Melillo G (2012). Overcoming disappointing results with antiangiogenic therapy by targeting hypoxia. Nat Rev Clin Oncol 9: 378–390.

Rock EP, Goodman V, Jiang JX, Mahjoob K, Verbois SL, Morse D *et al.* (2007). Food and Drug Administration drug approval summary: sunitinib malate for the treatment of gastrointestinal stromal tumor and advanced renal cell carcinoma. Oncologist 12: 107–113.

Rodamer M, Elsinghorst PW, Kinzig M, Gutschow M, Sorgel F (2011). Development and validation of a liquid chromatography/tandem mass spectrometry procedure for the quantification of sunitinib (SU11248) and its active metabolite, N-desethyl sunitinib (SU12662), in human plasma: application to an explorative study. J Chromatogr B Analyt Technol Biomed Life Sci 879: 695–706.

Roskoski R Jr (2007). Sunitinib: a VEGF and PDGF receptor protein kinase and angiogenesis inhibitor. Biochem Biophys Res Commun 356: 323–328.

Solon EG (2012). Use of radioactive compounds and autoradiography to determine drug tissue distribution. Chem Res Toxicol 25: 543–555.

Solon EG, Schweitzer A, Stoeckli M, Prideaux B (2010). Autoradiography, MALDI-MS, and SIMS-MS imaging in pharmaceutical discovery and development. AAPS J 12: 11–26.

Speed B, Bu HZ, Pool WF, Peng GW, Wu EY, Patyna S *et al.* (2012). Pharmacokinetics, distribution, and metabolism of [14C]sunitinib in rats, monkeys, and humans. Drug Metab Dispos 40: 539–555.

Strupat K, Kovtoun V, Bui H, Viner R, Stafford G, Horning S (2009). MALDI produced ions inspected with a linear ion trap-Orbitrap hybrid mass analyzer. J Am Soc Mass Spectrom 20: 1451–1463.

Sun L, Liang C, Shirazian S, Zhou Y, Miller T, Cui J *et al.* (2003). Discovery of 5-[5-fluoro-2-oxo-1,2- dihydroindol-(3Z)-ylidenemethyl]-2,4- dimethyl-1H-pyrrole-3-carboxylic acid (2-diethylaminoethyl)amide, a novel tyrosine kinase inhibitor targeting vascular endothelial and platelet-derived growth factor receptor tyrosine kinase. J Med Chem 46: 1116–1119.

Waldner MJ, Neurath MF (2012). Targeting the VEGF signaling pathway in cancer therapy. Expert Opin Ther Targets 16: 5–13.

Wong H, Choo EF, Alicke B, Ding X, La H, McNamara E *et al.* (2012). Antitumor activity of targeted and cytotoxic agents in murine subcutaneous tumor models correlates with clinical response. Clin Cancer Res 18: 3846–3855.

Xiao YY, Zhan P, Yuan DM, Liu HB, Lv TF, Song Y *et al.* (2013). Chemotherapy plus multitargeted antiangiogenic tyrosine kinase

inhibitors or chemotherapy alone in advanced NSCLC: a meta-analysis of randomized controlled trials. Eur J Clin Pharmacol 69: 151–159.

Zhou Q, Gallo JM (2010). Quantification of sunitinib in mouse plasma, brain tumor and normal brain using liquid chromatography-electrospray ionization-tandem mass spectrometry and pharmacokinetic application. J Pharm Biomed Anal 51: 958–964.

Supporting information

Additional Supporting Information may be found in the online version of this article at the publisher's web-site:

http://dx.doi.org/10.1111/bph.12990

Figure S1 After the MALDI-MSI analysis of tumour tissue sections, the matrix was washed off the slides with 70% ethanol and conventional haematoxylin and eosin (HE) staining was performed. Figure S1 shows the HE-stained section of the sunitinib-treated tumour shown in Figures 6B and C respectively.

Figure S2 HE-stained section of the control tumour shown in Figure 6C.